Imaging lutein and zeaxanthin in the human retina with confocal resonance Raman microscopy

Binxing Li[a], Evan W. George[a], Gregory T. Rognon[a], Aruna Gorusupudi[a], Arunkumar Ranganathan[a], Fu-Yen Chang[a], Linjia Shi[a], Jeanne M. Frederick[a], and Paul S. Bernstein[a,1]

[a]Department of Ophthalmology and Visual Sciences, Moran Eye Center, University of Utah School of Medicine, Salt Lake City, UT 84132

Edited by Janet R. Sparrow, Columbia University Medical Center, New York, NY, and accepted by Editorial Board Member Jeremy Nathans April 1, 2020 (received for review December 30, 2019)

Lutein and zeaxanthin are xanthophyll carotenoids that are highly concentrated in the human macula, where they protect the eye from oxidative damage and improve visual performance. Distinguishing lutein from zeaxanthin in images of the human retina in vivo or in donor eye tissues has been challenging because no available technology has been able to reliably differentiate between these two carotenoids, which differ only in the position of one C = C bond. Here, we report the differential distributions of lutein and zeaxanthin in human donor retinas mapped with confocal resonance Raman microscopy. Zeaxanthin is highly concentrated in the fovea, extending from the inner to the outer limiting membranes, with especially high concentrations in the outer plexiform layer, while lutein is much more diffuse at relatively lower concentration. Our results imply that zeaxanthin may play a more important role than lutein in human macular health and disease.

lutein | zeaxanthin | Raman | retina | macula

The *macula lutea* is an oval-shaped yellow region unique to the primate retina, which is responsible for sharp and detailed central vision (1–4). George Wald first recognized in 1945 that the yellow color of the macula originated from the deposition of xanthophyll carotenoids, presumably derived from the diet because animals cannot synthesize carotenoids (5). These xanthophyll carotenoids were chemically identified to be lutein and zeaxanthin by Bone and Landrum in 1985, and a few years later, they determined that lutein was exclusively in the *3R,3′R,6′R* configuration commonly found in plants and microorganisms, while zeaxanthin was a nearly equal mixture of dietary *3R,3′R*-zeaxanthin and nondietary *3R,3′S-meso*-zeaxanthin, with a very small amount of the nondietary *3S,3′S* isomer (6, 7). The P.S.B. laboratory and coworkers found that ∼20% of the macular pigment (MP) carotenoids are oxidation products of lutein and zeaxanthin and that *meso*-zeaxanthin is produced from lutein by the RPE65 enzyme in the retinal pigment epithelium (RPE) (8–11). In the peripheral retina, the ratio of lutein:zeaxanthin:*meso*-zeaxanthin is about 3:1:0 when measured by high-performance liquid chromatography (HPLC), while in the *macula lutea*, the concentration of total carotenoids rises 100-fold, and the ratio changes to 1:1:1 (12–16).

Snodderly studied the cross-sectional localization of the MP carotenoids in 1984 in sections of monkey retina using blue-light microscopy. At the fovea, the majority of the carotenoids were present in the outer plexiform layer and the inner plexiform layer, 2 of the 10 layers of the primate retina (17, 18). This focal distribution of macular carotenoids has been ascribed to the presence of specific binding proteins for the zeaxanthins (GSTP1) and lutein (StARD3) in the human macula (19–21). Besides being able to absorb short-wavelength blue light (1, 2, 4, 22), lutein and zeaxanthin are well-known natural antioxidants that can quench free radicals and singlet oxygen (23, 24). Furthermore, clinical studies have demonstrated that high macular pigment optical density (MPOD) is inversely associated with the risk of age-related macular degeneration (AMD), a common cause for blindness in developed countries and that carotenoid supplementation can reduce the risk of AMD and improve visual performance (25–33).

We and others have long had an interest in understanding how and why the primate macula goes to such great lengths to specifically concentrate lutein, zeaxanthin, and *meso*-zeaxanthin at the fovea. While it is possible to distinguish the differential distributions of lutein and the zeaxanthins on a macroscopic level by dissecting tissues, extracting, and analyzing by HPLC, such methods cannot provide microscopic resolution because tissue punches typically have to be several millimeters in diameter. Snodderly's blue light microscopic method on tissue sections fails to distinguish lutein from the zeaxanthins because their visible absorption spectra overlap too much, and other yellow chromophores may be present (17, 18). Other in situ methods such as fluorescence microscopy and imaging mass spectrometry likewise fail because carotenoids exhibit only weak fluorescence and could be easily destroyed by the conditions required for in situ mass spectrometry (34). On the other hand, the MP carotenoids exhibit strong, resonance-enhanced Raman spectra when excited with blue laser light even in complex tissue matrices (Fig. 1), and due to differences in carbon–carbon double-bond conjugation (10 for lutein and 11 for zeaxanthin and *meso*-zeaxanthin), they have subtly different but distinguishable Raman spectra (35, 36). In this study, we first optimized the conditions to distinguish lutein from the zeaxanthins using a high-resolution confocal resonance Raman microscope. Using these optimized methods, we separately measured the distributions of lutein and the zeaxanthins in human retinal sections and in Z-stack images of a flat-mounted human retina.

Significance

We have determined the spatial distribution of the macular pigment carotenoids lutein and zeaxanthin in the human retina using confocal resonance Raman microscopy and found that zeaxanthin is highly concentrated in the fovea, while lutein is more diffusely spread across the macula at a relatively lower concentration. Our results imply that zeaxanthin may play a more important role than lutein in human macular health and disease, and they demonstrate the elegant ability of confocal resonance Raman imaging to probe the biochemistry and structure of the most important region of the human retina.

Author contributions: B.L. and P.S.B. designed research; B.L., E.W.G., G.T.R., A.G., A.R., F.-Y.C., L.S., and J.M.F. performed research; B.L., A.G., A.R., J.M.F., and P.S.B. analyzed data; and B.L. and P.S.B. wrote the paper.

The authors declare no competing interest.

This article is a PNAS Direct Submission. J.R.S. is a guest editor invited by the Editorial Board.

[1]To whom correspondence may be addressed. Email: paul.bernstein@hsc.utah.edu.

This article contains supporting information online at https://www.pnas.org/lookup/suppl/doi:10.1073/pnas.1922793117/-/DCSupplemental.

First published May 14, 2020.

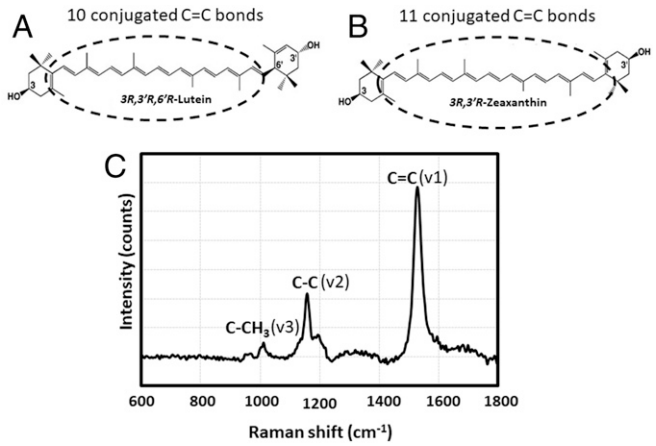

Fig. 1. Chemical structures and a typical Raman spectrum of macular carotenoids. (*A*) Lutein. (*B*) Zeaxanthin. (*C*) A Raman spectrum of zeaxanthin, demonstrating the typical Raman spectrum of a carotenoid. Three major peaks position at about 1,500 (v1), 1,150 (v2), and 1,000 cm^{-1} (v3). They originate from vibrations of conjugated C = C double bonds, C-C single bonds, and methyl groups in the carotenoid molecules, respectively. In theory, a carotenoid with longer C = C double-bond conjugation positions its v1 peak at a smaller Raman frequency, making it possible to distinguish lutein from zeaxanthin.

Results

Optimization of Raman Signal Acquisition. The total macular carotenoid concentration is about 1 mM at the fovea and drops to less than 10 μM in peripheral retina (1). To assess lower limits of sensitivity, we dissolved lutein and zeaxanthin standards in methanol at final concentrations of 0, 1, 5, and 10 μM and measured Raman spectra. *SI Appendix*, Fig. S1 shows that Raman spectra of even 1 μM carotenoid solutions are discernable and that the intensities of each of the three typical Raman peaks become stronger with increasing carotenoid concentration.

To optimize spectral resolution for the separation of the v1 peak of lutein from zeaxanthin, the Raman spectra of 10 μM lutein and 10 μM zeaxanthin in methanol were obtained using four different grating densities. Fig. 2 shows that the v1 peaks of lutein and zeaxanthin can be separated with 1,800 and 2,400 grooves/mm but not 600 or 1,200 grooves/mm. When the density of grating is set to 1,800 grooves/mm or 2,400 grooves/mm, the v1 peak of lutein is at 1,532 cm^{-1}, whereas that of zeaxanthin occurs at 1,528 cm^{-1}. Since the intensity of the Raman signal becomes smaller with increasing grating density, 1,800 grooves/mm was selected for all further measurements.

Next, we validated the ability of the Raman microscope to distinguish lutein from zeaxanthin using its built-in Classical Least Squares (CLS) algorithm. We prepared various 10-μM mixtures of lutein and zeaxanthin in methanol. Then, the contents of lutein and zeaxanthin in the mixture solutions were measured by Raman CLS fitting and by HPLC. Fig. 3 demonstrates that the proportion of lutein in the mixed carotenoid solutions determined by CLS fitting is highly correlated to the proportion detected by HPLC ($r = 0.997$, $P < 0.001$), indicating that the CLS algorithm is as reliable as HPLC for macular carotenoid quantification and identification.

Because most human macular carotenoids are thought to be bound to specific carotenoid-binding proteins, we also determined whether protein binding induces a spectral shift in the carotenoids' Raman spectra relative to carotenoids dissolved in a detergent that mimics lipid membranes. We used a ligand–protein binding method that we previously implemented to demonstrate that interactions of MP carotenoids with their binding proteins lengthen fluorescence decay lifetimes of protein-bound lutein and zeaxanthin relative to these carotenoids dissolved in detergent (37). Lutein, zeaxanthin, lutein-StARD3 protein complexes, and zeaxanthin-GSTP1 protein complexes were dissolved in phosphate buffered saline (PBS) buffer with 8 mM 3-[(3-Cholamidopropyl) dimethylammonio]-1-propanesulfonate hydrate (CHAPS), a zwitterionic detergent used to increase the aqueous solubility of carotenoids and carotenoid–protein complexes, and their Raman spectra were then measured. *SI Appendix*, Fig. S2 demonstrates that the overall spectra are unchanged, and the v1 peaks of lutein and zeaxanthin are still at 1,532 and 1,528 cm^{-1}, respectively, whether dissolved in detergent alone or bound to protein, although the signal intensity becomes weaker when they are bound to protein.

Resonance Raman Imaging of Macular Carotenoids in Tissue Sections. Using the optimized Raman methods, we first mapped the total carotenoids in a retinal section from a healthy donor eye with excitation from a 473-nm blue laser. The intensity map of total carotenoids was created using the peak intensity of each Raman spectra of the v1 peak between 1,500 and 1,550 cm^{-1} in a region 1,800 μm × 500 μm centered at the foveal pit. Fig. 4 shows that most carotenoids localize to the 700-μm-wide foveal depression with a steep drop to barely detectable levels more peripherally. Cross-sectionally at the foveal center, the strongest Raman signals were detected in the OPL (also known as Henle's fiber layer) and the ONL.

Fig. 5 shows the Raman spectra at various selected points on the Raman intensity map of Fig. 4. All three spots in the inner retina exhibit a typical carotenoid spectrum, with the spot at the center showing the strongest Raman intensity and progressively weaker signals with increasing distance from the fovea. The foveal ONL also manifests a strong and clear Raman spectrum typical for carotenoids, which diminishes to undetectable levels just a few hundred microns (μm) from the foveal center. Interestingly, carotenoids are not detectable in photoreceptor outer segments anywhere in the macula. Strong background fluorescence was present in the RPE layer, presumably from lipofuscin, which likely overwhelms any weak Raman signals originating from the low concentrations of carotenoids known to be present in the RPE by HPLC analysis (38–40).

Next, we mapped the distributions of lutein and zeaxanthin separately based on the intensity map of total carotenoids shown in Fig. 6*A*. To do so, the CLS application in the LabSpec6 software was employed to distinguish lutein from zeaxanthin using the Raman spectra of lutein and zeaxanthin of Fig. 2*C* as the references. The distribution of zeaxanthin closely matches the pattern of total carotenoids concentrated in the fovea with dramatically reduced concentrations in the peripheral regions (Fig. 6*B*). In contrast with zeaxanthin, lutein is spread throughout the entire section at low concentration (Fig. 6*C*). These data were replotted in *SI Appendix*, Fig. S3 showing the distributions of total carotenoids, lutein, and zeaxanthin as horizontal cuts at depths corresponding to the labels in Fig. 6*A*. From the inner to the outer retina, the intensity of total carotenoids increased progressively from GCL to OPL, was at substantial concentrations in the ONL only in the foveal center, and then dropped to very low levels in the OS and RPE. At the very center of the fovea, there are no detectable carotenoids in the GCL, IPL, and INL cuts because these layers are not present in the foveal pit. The zeaxanthin distribution corresponds well to the distribution of total carotenoids, especially in layers with the highest total carotenoid concentrations (OPL and ONL), where its concentration far exceeds that of lutein. Lutein is distributed across every retinal layer except for a small increase in concentration at the surface of the foveal pit, where its ratio to zeaxanthin may exceed 1:1.

To determine if the above results obtained from the first donor are reproducible, we next measured carotenoids in sections from another donor's eye in a comparable manner. *SI Appendix*, Fig. S4 shows a section near the foveal center, which displays a

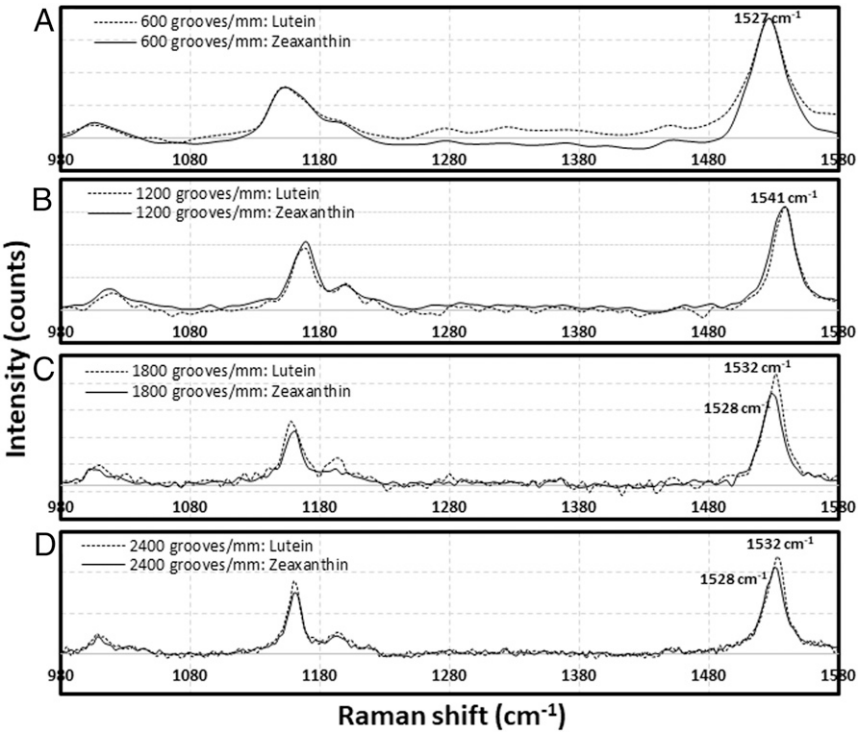

Fig. 2. Optimization of acquisition conditions for confocal resonance Raman microscopy to distinguish zeaxanthin from lutein. Zeaxanthin and lutein standards were dissolved in methanol at 10-μM concentrations. Of four Raman gratings, (*A*) 600, (*B*) 1,200, (*C*) 1,800, and (*D*) 2,400 grooves/mm, the 1,800 and 2,400 grooves/mm gratings were the best. The Raman shifts of the peaks of the C = C bond vibrations of zeaxanthin and lutein were distinguishable at 1,528 and 1,532 cm^{-1}, respectively.

total carotenoid distribution pattern similar to the one seen in Fig. 4, with the highest concentrations in the OPL and ONL, but with a narrower foveal depression and a broader carotenoid distribution. In addition, avulsed inner limiting membrane (ILM) was observed, and a strong Raman carotenoid signal was detected in this structure, too. Once again, zeaxanthin is the predominant foveal carotenoid with a distribution that closely matches the total carotenoid map, but unlike the first donor's eye, this donor's lutein map does correspond reasonably well with the total carotenoid distribution, albeit at a lower level than zeaxanthin. *SI Appendix*, Fig. S5, a section cut ~40 μm from the foveal center (*SI Appendix*, Fig. S4), reveals a lower signal for total carotenoids, which is completely depleted in the ONL. Unlike the foveal section, the concentrations of lutein and zeaxanthin are very similar, but lutein still has a broader distribution than zeaxanthin. The Raman spectra of total carotenoids, lutein, and zeaxanthin at two selected locations (white squares in *SI Appendix*, Fig. S5*B*) are shown in *SI Appendix*, Fig. S5 *F* and *G*. The intensity of lutein's Raman spectrum is about four times higher than zeaxanthin's at spot F, and this ratio is reversed at spot G, just 200 μm closer to the fovea.

Resonance Raman Imaging of Macular Carotenoids in a Flat-Mounted Retina. We also imaged carotenoids in a flat-mounted 8-mm macular punch from another healthy donor eye (Fig. 7), which was placed on a microscope slide with the vitreous side up and RPE side down (see top left inset). Next, a Z-stack map of total carotenoids in a 1 × 1-mm square centered at the fovea was created from the surface of the retina to 300 μm depth with offset steps of 50 μm. Thus, seven 1 × 1-mm optical section maps of total carotenoids were obtained along the Z-direction, corresponding roughly to each of the retinal layers. In Fig. 7, a ring-shaped distribution of carotenoids is seen in the GCL, IPL, and INL, while the carotenoid distribution in the OPL and ONL appears as a disk, and the OS has barely detectable carotenoids. The width of the carotenoid rings and disks becomes smaller with increasing depth, and signal intensity peaks in the OPL. We then generated the maps of lutein and zeaxanthin in these seven retinal layers using the instrument's CLS algorithm (Fig. 8). Zeaxanthin's distribution pattern is similar to the total carotenoids, with the strongest signals in the IPL, INL, OPL, and ONL, while lutein's signal is almost undetectable at the same intensity scale. When the scale bar is expanded 10-fold, the Raman signal of lutein is detectable in

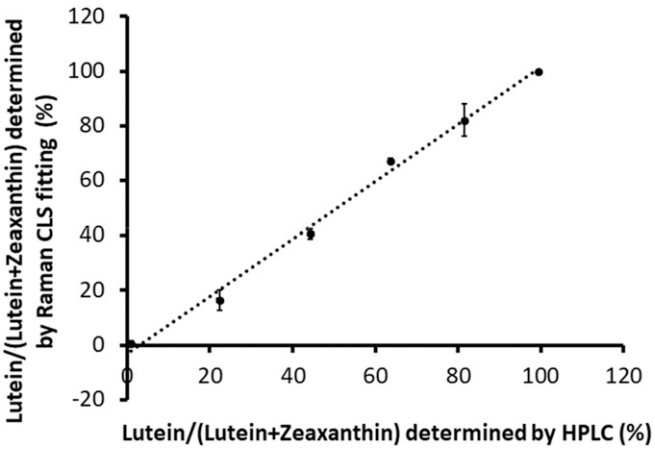

Fig. 3. Comparison of the ability to distinguish lutein from zeaxanthin using the Raman microscope's CLS algorithm or HPLC. To determine the relative accuracies of the Raman CLS algorithm and HPLC to separate lutein and zeaxanthin, 10-μM methanolic mixtures of lutein and zeaxanthin were prepared and analyzed by Raman spectroscopy with CLS fitting and by HPLC. Our data demonstrate that the Raman CLS algorithm performed as well as HPLC ($r^2 = 0.9971$, $P < 0.001$). Each data point represents the mean of three different replicate experiments, and the error bars indicate SDs.

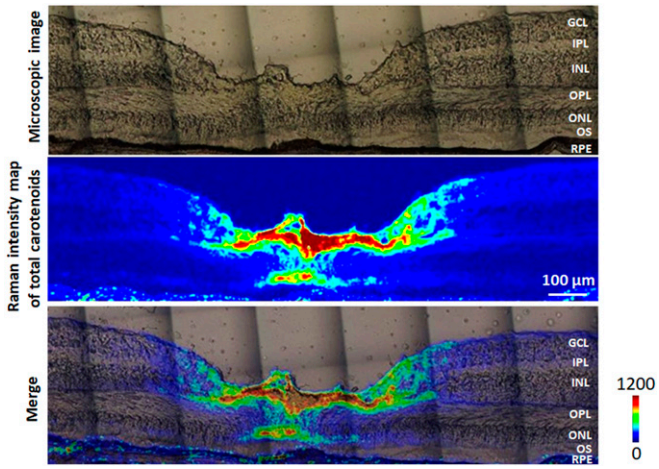

Fig. 4. Distribution of total carotenoids in a human retinal section. (*Top*) A microscopic image of a retinal section from a healthy 77-year-old female donor. (*Middle*) Intensity map of total carotenoids created using Raman signal in a 1,500 to 1,550 cm^{-1} window. (*Bottom*) Overlay of the total carotenoid map on the microscopic image. GCL, ganglion cell layer; IPL, inner plexiform layer; INL, inner nuclear layer; OPL, outer plexiform layer; ONL, outer nuclear layer; OS, outer segment; RPE, retinal pigment epithelium.

these four layers, but unlike zeaxanthin, the lutein distribution exhibits minimal spatial specificity.

Discussion

We have generated high-resolution differential distribution maps of lutein and zeaxanthin in the human retina in situ using confocal resonance Raman microscopy. Our results demonstrate that zeaxanthin mainly accumulates in the IPL, OPL, and ONL at the center of the human foveal pit, while lutein is distributed more diffusely across the retina at a much lower concentration relative to zeaxanthin, suggesting that zeaxanthin is more important than lutein as the foveal MP.

Our maps of human total carotenoids are consistent with the light-microscopy map of macular pigments in monkey retinal sections published by Snodderly et al. in which most carotenoids were concentrated in the primate macular OPL and IPL (18); however, we also see that carotenoids localized to the ONL of the human foveola, a 300-μm region centered at the foveal pit (Fig. 4 and *SI Appendix*, Fig. S4). Fig. 4 is remarkable because the total carotenoids display a bouquet shape in the foveal avascular zone, roughly 800 μm wide in the inner retina, narrowing to 150 μm at the OPL/ONL junction, and then flaring out to 300 μm at the outer limiting membrane (OLM). *SI Appendix*, Fig. S4 shows similar narrowing at the ONL without widening at the OLM, possibly because this section is not exactly at the center of the foveal pit. These bouquet or inverted cone-like features are corroborated by the Z-stack image of total carotenoids (Fig. 7), in which the ring-shaped or disk-shaped distribution patterns of total carotenoids in each successive retinal layer shrink in diameter with increasing depth from the inner to the outer retina. These patterns are consistent with carotenoid localization within the Müller cell cone which terminates at the OLM, a hypothesis first advanced by Gass (41) and supported by studies on macular telangiectasia type 2 (MacTel) eyes in which Müller cell loss coincides with MP depletion and redistribution (42–44). We cannot rule out that the MP carotenoids are found in the foveal photoreceptor axons (Henle fibers) as well, especially since immunohistochemistry localizes GSTP1 and StARD3 to Henle fibers rather than Müller cells (19, 21). Future immunohistochemistry/Raman studies at higher resolution should be able to provide further insights on the relative distributions of MP carotenoids and their binding proteins in foveal photoreceptors and Müller cells.

We also detected strong carotenoid Raman signals in avulsed ILM (*SI Appendix*, Figs. S4 and S5). This corresponds nicely with Obana's report of MP presence in surgically removed lamellar hole-associated epiretinal proliferation in patients with lamellar macular hole (45). ILM and lamellar hole-associated epiretinal proliferation are both thought to be of Müller cell origin, further supporting a key role of foveal Müller cells in carotenoid deposition.

The spatial distributions of zeaxanthin and lutein were separately imaged in the human retina in situ. We found that, like the total carotenoids, zeaxanthin accumulates in the fovea at very high concentration and drops sharply in the periphery of the macula. In contrast, lutein is distributed across the macula more

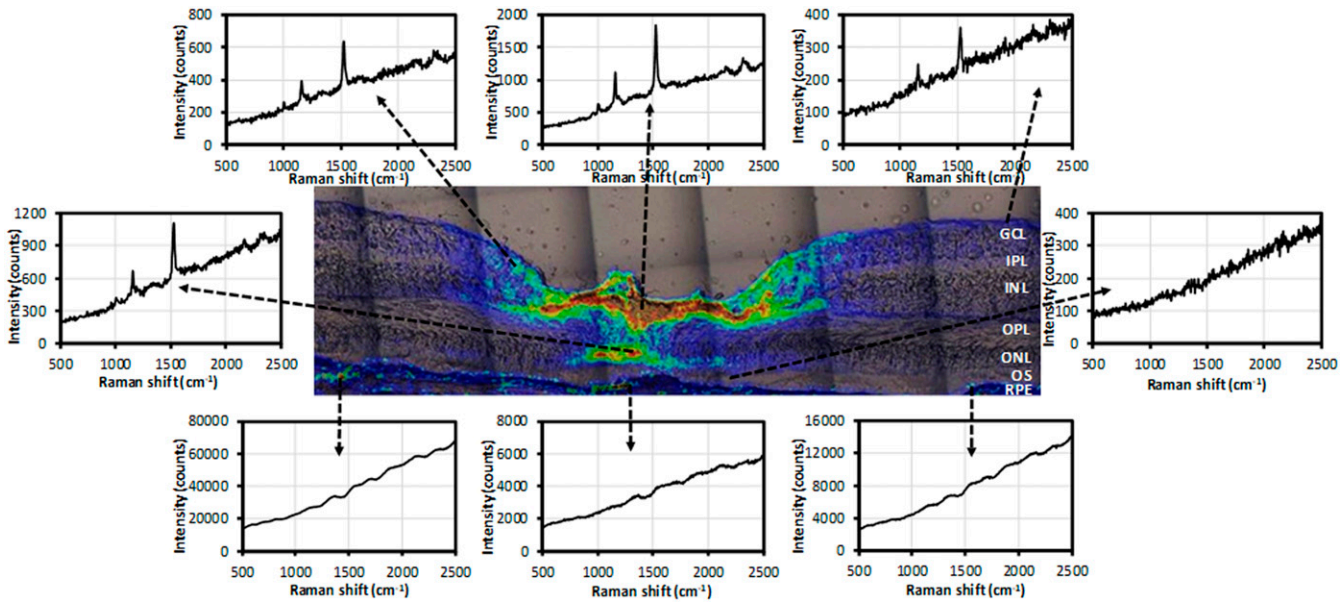

Fig. 5. Raman spectra at selected locations in the intensity map of total carotenoids. Three spots from the surface of the retina, one from the foveal ONL, one from the foveal OS, and three from RPE were selected from the image shown in Fig. 4.

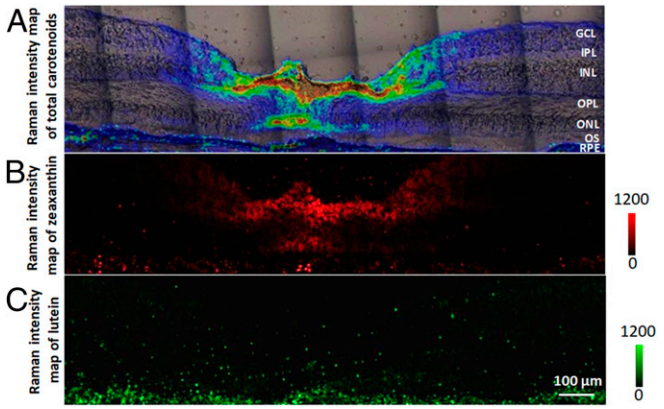

Fig. 6. Distributions of zeaxanthin and lutein in a human retinal section. (*A*) An overlaid image of the total carotenoid map and microscopic image originally shown in Fig. 4. (*B*) An intensity map of zeaxanthin generated using CLS fitting. (*C*) An intensity map of lutein generated using CLS fitting.

evenly at lower concentrations. Quantitatively, the zeaxanthin:lutein ratio decreases with increasing eccentricity from the fovea. We found that zeaxanthin:lutein ratio can be greater than 9:1 at the foveal center, is about 4:1 at a spot around 200 μm away, and inverts to about 1:4 200 μm further (Fig. 6 and *SI Appendix*, Figs. S4 and S5). These results demonstrate the power of the confocal resonance Raman technique to map MP carotenoid distributions at far higher resolution than the previously reported 2:1 foveal zeaxanthin:lutein ratio reported in HPLC-based studies.

The mechanism and physiological significance of the selective concentration of zeaxanthin over lutein in the primate fovea remains inadequately explained, however. Previously, we found that the MPOD of newborns is significantly associated with the serum zeaxanthin level of their mothers, while serum lutein is not (46). Clinical research has demonstrated that MPOD is inversely associated with AMD risk, and there is some evidence that supplementation with mixed carotenoids may be superior to lutein alone (47, 48). The fovea is a region at high risk for light-induced oxidative stress from reactive oxygen species and singlet oxygen that can be generated by A2E, A2PE, and other bis-retinoid components of lipofuscin, and zeaxanthin is capable of quenching more singlet oxygen than lutein in ocular tissues and in biochemical assays (24, 49). More recently, we found that zeaxanthin supplementation improves the visual performance of mice better than lutein (32). Therefore, the preferential selection of zeaxanthin at the fovea may better facilitate this macular region's role to provide high-acuity vision while resisting oxidative damage. Although *meso*-zeaxanthin can be synthesized from dietary lutein by RPE65 in the RPE, this reaction appears to be relatively slow and inefficient. Our results lend support for considering higher levels of zeaxanthin and/or *meso*-zeaxanthin supplementation beyond the current AREDS2 formula's 10 mg of lutein and 2 mg of zeaxanthin.

The differential distributions of lutein and zeaxanthin in the human retina revealed in this work may enhance our understanding of the uptake and transport mechanism of macular carotenoids. It is already known that the specific distributions of lutein and zeaxanthin in the human retina are in part explained by their binding proteins StARD3 and GSTP1 (19, 21). In this study, we conclusively demonstrated that zeaxanthin is highly concentrated in the fovea, while lutein is much more diffusely distributed (Fig. 6 and *SI Appendix*, Figs. S4 and S5). Humans do not have the enzymes to synthesize carotenoids and must obtain them from the diet, implying that the macular carotenoids must come from the circulation. Since the fovea is avascular, it is likely that its zeaxanthin comes in from the choroidal circulation via the RPE either as dietary *3R,3′R*-zeaxanthin or as *3R,3′S-meso*-zeaxanthin produced from dietary lutein by RPE65 in the RPE (11). A recent study reported that high-density lipoprotein (HDL) is the main transporter for zeaxanthin, and since our results indicate that >90% of the carotenoids in the fovea can be zeaxanthin, this indicates that a large proportion of the macular carotenoids influxes into the retina through RPE via RPE65 and HDL (50). It has also been reported that genetic mutants of many HDL receptors and proteins, such as SR-BI, ABCA1, Apo A1, and Apo E, are associated with retinal carotenoid levels (51–53). Lutein, on the other hand, has a much more diffuse distribution across the retina and could come in through the retinal circulation as well.

There are several limitations to this study. First, we cannot separate *3R,3′R*-zeaxanthin from *3R,3′S-meso*-zeaxanthin because they have identical Raman spectra. Second, the results of this study were obtained from a small number of donor eyes. Therefore, our findings need to be expanded to include tissues from a variety of donors, with and without macular pathology, but it is challenging to get human donor eyes suitable for the Raman

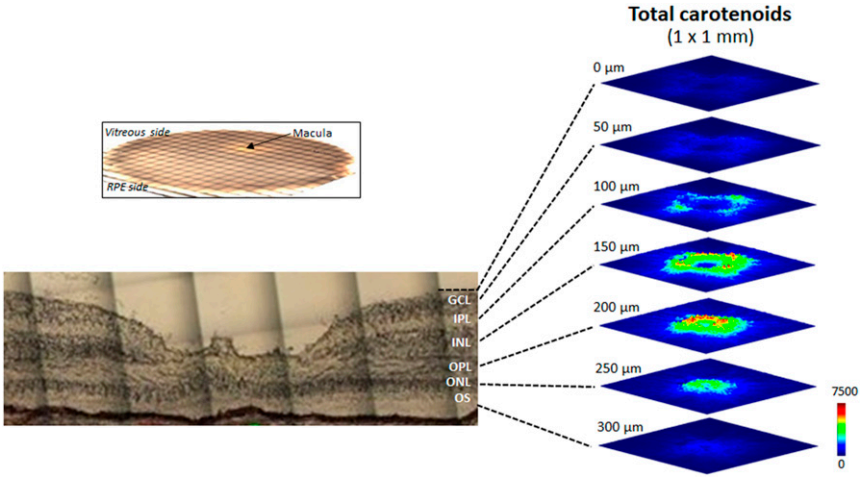

Fig. 7. Z-stack images of total carotenoids in a flat-mounted human retina. The arrow shows the *macula lutea* of an 8-mm macular punch from a healthy 86-year-old male donor. Total carotenoids in a 1 × 1-mm square centered at the fovea were imaged from the vitreal surface to the outer segment layer every 50 μm, yielding seven images to a depth of 300 μm. The light microscopic image at the lower left is from a different donor eye and is provided for orientation purposes only.

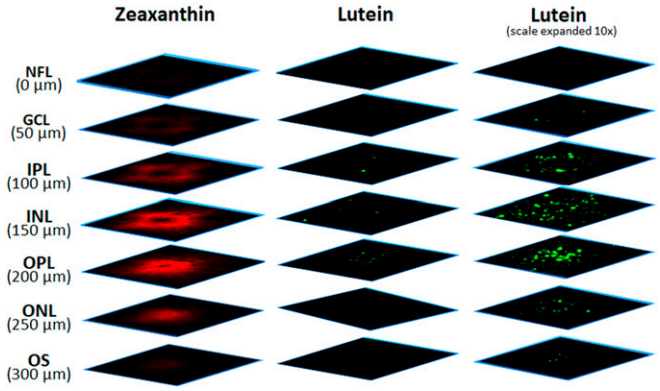

Fig. 8. Z-stack images of lutein and zeaxanthin in a flat-mounted human retina. Using CLS fitting, the total carotenoids in Fig. 7 were further divided into zeaxanthin and lutein maps. (*Left* column) The intensity map of zeaxanthin. (*Center* column) The intensity map of lutein. (*Right* column) The intensity map of lutein with the scale expanded 10 times. NFL, nerve fiber layer.

measurement, and even a single confocal Raman image can take hours or days to acquire.

In conclusion, using confocal resonance Raman microscopy, we measured the differential distributions of lutein and zeaxanthin in the human retina and found that zeaxanthin is localized to the foveal center at high concentrations from the ILM to the OLM, while lutein is diffusely distributed across the inner retina at a much lower concentration. Our results support the hypotheses that zeaxanthin is more important than lutein as the foveal MP and that the Müller cell cone is a reservoir for MP. We anticipate that further confocal resonance Raman studies of macular pigment will provide additional insights on the unique role of the MP carotenoids in retinal health and disease.

Materials and Methods

Chemicals, Reagents, and Proteins Used in the Optimization Assays. Lutein and zeaxanthin standards were obtained from Kemin Health and ZeaVision, respectively. All carotenoids were crystalline, and their purities were >98%. CHAPS was purchased from Sigma-Aldrich. The carotenoid standards were dissolved either in methanol or 0.1 M PBS containing 8 mM CHAPS. Lutein-binding protein (StARD3) and zeaxanthin-binding protein (GSTP1) were expressed in *Escherichia coli* and purified as described (21, 54, 55) and dissolved in PBS containing 8 mM CHAPS. Carotenoid–protein complexes of lutein–StARD3 and zeaxanthin–GSTP1 were prepared using reported methods (37, 56). Then, the solutions of carotenoids and carotenoid-binding proteins were put into a 2-mm path length quartz cuvette for spectroscopic measurements. Carotenoid and protein concentrations were determined using a SmartSpec 3000 spectrophotometer (Bio-Rad). For the detailed methods of HPLC analysis, please see *SI Appendix*.

Preparation of Flat-Mounted Retinas and Retinal Sections. Human donor eyes were provided by the Utah Lions Eye Bank. The eyes were collected within 6 h of death and fixed by immersion in 4% paraformaldehyde in PBS for 1 h at room temperature. Following removal of the anterior segments, 8-mm macular punches were washed in PBS and either flat-mounted on a quartz slide or processed further for retinal sections. For retinal sections, the washed macular punches were infiltrated with 15% sucrose in PBS for 1 to 2 h and then in 30% sucrose in PBS overnight at 4 °C in darkness. Subsequently, the macular punches were embedded in Tissue-Tek O.C.T. compound (Sakura Finetek USA, Inc.), frozen, and transversely sectioned at 12-μm thickness. All slide-mounted retinal sections were kept in a −80 °C freezer until use.

Confocal Resonance Raman Microscopy. Resonance Raman signals of carotenoids were acquired using an XploRA Plus confocal Raman microscope (Horiba Instruments Inc.). This confocal Raman microscope includes an Olympus BX-41 microscope and an XploRA Plus Raman imaging spectrometer, which is coupled with a computer-controlled XYZ motorized stage, and a computer-controlled heating and cooling stage (LINK-PE120). All measurements and data analyses were controlled by Horiba LabSpec6 software. To perform the optimization assays, a Macro cuvette cell sample holder was first attached to the microscope turret. Then, the carotenoid solutions were added into the quartz cuvette and put into the holder. Raman spectra were detected with excitation from a 473-nm blue laser at room temperature. To image the total carotenoids in the human retinal sections and flat-mounted retinas, the same 473-nm laser was also employed, and all of the samples were mounted on the cooling stage at a holding temperature of 4 °C during Raman imaging. The parameters of instrument and acquisition were set as follows: 10× or 20× microscope objective lens, 3.5 mW laser power; 1,800 grooves/mm grating; 50 μm slit; 100 μm confocal pinhole; 1.0 second acquisition time per voxel. The step sizes along X- and Y- axes were set to 5 μm when mapping retinal sections, and they were set to 10 μm when mapping the flat-mounted retina. The minimum step sizes for the computer-controlled XY motorized stage and Z-motor are 0.1 and 0.5 μm, respectively. Intensity maps of total carotenoids were created by mapping the intensity of the v1 Raman peak measured in a 1,500 to 1,550 cm^{-1} window. Separate lutein and zeaxanthin intensity maps were prepared with the LabSpec6 software's CLS fitting procedure using the Raman spectra of standard lutein and zeaxanthin in methanol as references.

Data Availability Statement. All data discussed in the paper are available in the main text or *SI Appendix*.

ACKNOWLEDGMENTS. We thank Drs. Eunah Lee and David Tushel from Horiba Scientific Inc. (Edison, NJ) for their helpful technical support. This work was supported by NIH grants EY-11600 and EY-14800, by the Lowy Medical Research Institute, by the Carl Marshall & Mildred Almen Reeves Foundation, by the BrightFocus Foundation, and by unrestricted departmental funds from Research to Prevent Blindness, New York.

1. N. I. Krinsky, J. T. Landrum, R. A. Bone, Biologic mechanisms of the protective role of lutein and zeaxanthin in the eye. *Annu. Rev. Nutr.* **23**, 171–201 (2003).
2. S. Beatty, M. Boulton, D. Henson, H. H. Koh, I. J. Murray, Macular pigment and age related macular degeneration. *Br. J. Ophthalmol.* **83**, 867–877 (1999).
3. J. M. Provis, P. L. Penfold, E. E. Cornish, T. M. Sandercoe, M. C. Madigan, Anatomy and development of the macula: Specialisation and the vulnerability to macular degeneration. *Clin. Exp. Optom.* **88**, 269–281 (2005).
4. P. S. Bernstein *et al*., Lutein, zeaxanthin, and *meso*-zeaxanthin: The basic and clinical science underlying carotenoid-based nutritional interventions against ocular disease. *Prog. Retin. Eye Res.* **50**, 34–66 (2016).
5. G. Wald, Human vision and the spectrum. *Science* **101**, 653–658 (1945).
6. R. A. Bone, J. T. Landrum, S. L. Tarsis, Preliminary identification of the human macular pigment. *Vision Res.* **25**, 1531–1535 (1985).
7. R. A. Bone, J. T. Landrum, G. W. Hime, A. Cains, J. Zamor, Stereochemistry of the human macular carotenoids. *Invest. Ophthalmol. Vis. Sci.* **34**, 2033–2040 (1993).
8. A. Gorusupudi *et al*., Developmentally regulated production of *meso*-zeaxanthin in chicken retinal pigment epithelium/choroid and retina. *Invest. Ophthalmol. Vis. Sci.* **57**, 1853–1861 (2016).
9. P. S. Bernstein *et al*., Identification and quantitation of carotenoids and their metabolites in the tissues of the human eye. *Exp. Eye Res.* **72**, 215–223 (2001).
10. F. Khachik, F. F. de Moura, D. Y. Zhao, C. P. Aebischer, P. S. Bernstein, Transformations of selected carotenoids in plasma, liver, and ocular tissues of humans and in nonprimate animal models. *Invest. Ophthalmol. Vis. Sci.* **43**, 3383–3392 (2002).
11. R. Shyam, A. Gorusupudi, K. Nelson, M. P. Horvath, P. S. Bernstein, RPE65 has an additional function as the lutein to *meso*-zeaxanthin isomerase in the vertebrate eye. *Proc. Natl. Acad. Sci. U.S.A.* **114**, 10882–10887 (2017).
12. R. A. Bone, J. T. Landrum, L. Fernandez, S. L. Tarsis, Analysis of the macular pigment by HPLC: Retinal distribution and age study. *Invest. Ophthalmol. Vis. Sci.* **29**, 843–849 (1988).
13. R. A. Bone, J. T. Landrum, Z. Dixon, Y. Chen, C. M. Llerena, Lutein and zeaxanthin in the eyes, serum and diet of human subjects. *Exp. Eye Res.* **71**, 239–245 (2000).
14. P. Bhosale, D. Y. Zhao, P. S. Bernstein, HPLC measurement of ocular carotenoid levels in human donor eyes in the lutein supplementation era. *Invest. Ophthalmol. Vis. Sci.* **48**, 543–549 (2007).
15. F. Khachik, P. S. Bernstein, D. L. Garland, Identification of lutein and zeaxanthin oxidation products in human and monkey retinas. *Invest. Ophthalmol. Vis. Sci.* **38**, 1802–1811 (1997).
16. F. Khachik *et al*., Chemistry, distribution, and metabolism of tomato carotenoids and their impact on human health. *Exp. Biol. Med. (Maywood)* **227**, 845–851 (2002).
17. D. M. Snodderly, P. K. Brown, F. C. Delori, J. D. Auran, The macular pigment. I. Absorbance spectra, localization, and discrimination from other yellow pigments in primate retinas. *Invest. Ophthalmol. Vis. Sci.* **25**, 660–673 (1984).
18. D. M. Snodderly, J. D. Auran, F. C. Delori, The macular pigment. II. Spatial distribution in primate retinas. *Invest. Ophthalmol. Vis. Sci.* **25**, 674–685 (1984).
19. P. Bhosale *et al*., Identification and characterization of a Pi isoform of glutathione S-transferase (GSTP1) as a zeaxanthin-binding protein in the macula of the human eye. *J. Biol. Chem.* **279**, 49447–49454 (2004).

20. P. Bhosale *et al*., Purification and partial characterization of a lutein-binding protein from human retina. *Biochemistry* **48**, 4798–4807 (2009).
21. B. Li, P. Vachali, J. M. Frederick, P. S. Bernstein, Identification of StARD3 as a lutein-binding protein in the macula of the primate retina. *Biochemistry* **50**, 2541–2549 (2011).
22. A. J. Whitehead, J. A. Mares, R. P. Danis, Macular pigment: A review of current knowledge. *Arch. Ophthalmol.* **124**, 1038–1045 (2006).
23. N. I. Krinsky, Antioxidant functions of carotenoids. *Free Radic. Biol. Med.* **7**, 617–635 (1989).
24. B. Li, F. Ahmed, P. S. Bernstein, Studies on the singlet oxygen scavenging mechanism of human macular pigment. *Arch. Biochem. Biophys.* **504**, 56–60 (2010).
25. J. T. Landrum *et al*., A one year study of the macular pigment: The effect of 140 days of a lutein supplement. *Exp. Eye Res.* **65**, 57–62 (1997).
26. J. M. Seddon *et al*., Dietary carotenoids, vitamins A, C, and E, and advanced age-related macular degeneration. Eye Disease Case-Control Study Group. *JAMA* **272**, 1413–1420 (1994).
27. P. S. Bernstein *et al*., Resonance Raman measurement of macular carotenoids in normal subjects and in age-related macular degeneration patients. *Ophthalmology* **109**, 1780–1787 (2002).
28. Age-Related Eye Disease Study 2 Research Group, Lutein + zeaxanthin and omega-3 fatty acids for age-related macular degeneration: The Age-Related Eye Disease Study 2 (AREDS2) randomized clinical trial. *JAMA* **309**, 2005–2015 (2013).
29. Y. Yao *et al*., Lutein supplementation improves visual performance in Chinese drivers: 1-year randomized, double-blind, placebo-controlled study. *Nutrition* **29**, 958–964 (2013).
30. J. M. Stringham, B. R. Hammond, Macular pigment and visual performance under glare conditions. *Optom. Vis. Sci.* **85**, 82–88 (2008).
31. K. O. Akuffo *et al*., The impact of supplemental antioxidants on visual function in nonadvanced age-related macular degeneration: A head-to-head randomized clinical trial. *Invest. Ophthalmol. Vis. Sci.* **58**, 5347–5360 (2017).
32. B. Li *et al*., Supplementation with macular carotenoids improves visual performance of transgenic mice. *Arch. Biochem. Biophys.* **649**, 22–28 (2018).
33. B. R. Hammond, Jr, B. R. Wooten, J. Curran-Celentano, Carotenoids in the retina and lens: Possible acute and chronic effects on human visual performance. *Arch. Biochem. Biophys.* **385**, 41–46 (2001).
34. M. Sharifzadeh, A. Obana, Y. Gohto, T. Seto, W. Gellermann, Autofluorescence imaging of macular pigment: Influence and correction of ocular media opacities. *J. Biomed. Opt.* **19**, 96010 (2014).
35. P. S. Bernstein, M. D. Yoshida, N. B. Katz, R. W. McClane, W. Gellermann, Raman detection of macular carotenoid pigments in intact human retina. *Invest. Ophthalmol. Vis. Sci.* **39**, 2003–2011 (1998).
36. A. A. Arteni *et al*., Structure and conformation of the carotenoids in human retinal macular pigment. *PLoS One* **10**, e0135779 (2015).
37. L. Sauer *et al*., Fluorescence lifetime imaging ophthalmoscopy (FLIO) of macular pigment. *Invest. Ophthalmol. Vis. Sci.* **59**, 3094–3103 (2018).
38. J. R. Sparrow, K. Nakanishi, C. A. Parish, The lipofuscin fluorophore A2E mediates blue light-induced damage to retinal pigmented epithelial cells. *Invest. Ophthalmol. Vis. Sci.* **41**, 1981–1989 (2000).
39. R. K. Crouch, Y. Koutalos, M. Kono, K. Schey, Z. Ablonczy, A2E and lipofuscin. *Prog. Mol. Biol. Transl. Sci.* **134**, 449–463 (2015).
40. P. Bhosale, B. Serban, P. S. Bernstein, Retinal carotenoids can attenuate formation of A2E in the retinal pigment epithelium. *Arch. Biochem. Biophys.* **483**, 175–181 (2009).
41. J. D. Gass, Müller cell cone, an overlooked part of the anatomy of the fovea centralis: Hypotheses concerning its role in the pathogenesis of macular hole and foveomacualr retinoschisis. *Arch. Ophthalmol.* **117**, 821–823 (1999).
42. P. Charbel Issa *et al*., Macular telangiectasia type 2. *Prog. Retin. Eye Res.* **34**, 49–77 (2013).
43. M. B. Powner *et al*., Perifoveal Müller cell depletion in a case of macular telangiectasia type 2. *Ophthalmology* **117**, 2407–2416 (2010).
44. T. Zhang *et al*., Human macular Müller cells rely more on serine biosynthesis to combat oxidative stress than those from the periphery. *eLife* **8**, e43598 (2019).
45. A. Obana *et al*., Evidence of carotenoid in surgically removed lamellar hole-associated epiretinal proliferation. *Invest. Ophthalmol. Vis. Sci.* **58**, 5157–5163 (2017).
46. B. S. Henriksen *et al*., Interrelationships between maternal carotenoid status and newborn infant macular pigment optical density and carotenoid status. *Invest. Ophthalmol. Vis. Sci.* **54**, 5568–5578 (2013).
47. J. Loughman *et al*., The impact of macular pigment augmentation on visual performance using different carotenoid formulations. *Invest. Ophthalmol. Vis. Sci.* **53**, 7871–7880 (2012).
48. S. Sabour-Pickett *et al*., Supplementation with three different macular carotenoid formulations in patients with early age-related macular degeneration. *Retina* **34**, 1757–1766 (2014).
49. S. R. Kim, K. Nakanishi, Y. Itagaki, J. R. Sparrow, Photooxidation of A2-PE, a photoreceptor outer segment fluorophore, and protection by lutein and zeaxanthin. *Exp. Eye Res.* **82**, 828–839 (2006).
50. S. E. Thomas, E. H. Harrison, Mechanisms of selective delivery of xanthophylls to retinal pigment epithelial cells by human lipoproteins. *J. Lipid Res.* **57**, 1865–1878 (2016).
51. G. J. McKay *et al*., Investigation of genetic variation in scavenger receptor class B, member 1 (SCARB1) and association with serum carotenoids. *Ophthalmology* **120**, 1632–1640 (2013).
52. K. J. Meyers *et al*., Genetic determinants of macular pigments in women of the Carotenoids in Age-Related Eye Disease Study. *Invest. Ophthalmol. Vis. Sci.* **54**, 2333–2345 (2013).
53. K. J. Meyers *et al*., Genetic evidence for role of carotenoids in age-related macular degeneration in the Carotenoids in Age-Related Eye Disease Study (CAREDS). *Invest. Ophthalmol. Vis. Sci.* **55**, 587–599 (2014).
54. P. Vachali, B. Li, K. Nelson, P. S. Bernstein, Surface plasmon resonance (SPR) studies on the interactions of carotenoids and their binding proteins. *Arch. Biochem. Biophys.* **519**, 32–37 (2012).
55. B. Li *et al*., Inactivity of human β,β-carotene-9′,10′-dioxygenase (BCO2) underlies retinal accumulation of the human macular carotenoid pigment. *Proc. Natl. Acad. Sci. U.S.A.* **111**, 10173–10178 (2014).
56. P. Bhosale, P. S. Bernstein, Synergistic effects of zeaxanthin and its binding protein in the prevention of lipid membrane oxidation. *Biochim. Biophys. Acta* **1740**, 116–121 (2005).